REPORT DOCUMENTATION PAGE	Form Approved OMB No. 0704-0188

1. AGENCY USE ONLY (*LEAVE BLANK*)	2. REPORT DATE	3. REPORT TYPE AND DATES COVERED
	15 April 1996	Professional Paper

4. TITLE AND SUBTITLE
Validation and Application of a Transient Aeroelastic Analysis for Shipboard Engage/Disengage Operations

5. FUNDING NUMBERS

6. AUTHOR(S)
William P. Geyer, Jr.
Edward C. Smith
Jonathan Keller

7. PERFORMING ORGANIZATION NAME(S) AND ADDRESS(ES)
Commander
Naval Air Warfare Center Aircraft Division
22541 Millstone Road
Patuxent River, Maryland 20670-5304

8. PERFORMING ORGANIZATION REPORT NUMBER

9. SPONSORING/MONITORING AGENCY NAME(S) AND ADDRESS(ES)
Naval Air Systems Command
Department of the Navy
1421 Jefferson Davis Highway
Arlington, VA 22243

10. SPONSORING/MONITORING AGENCY REPORT NUMBER

11. SUPPLEMENTARY NOTES

12a. DISTRIBUTION/AVAILABILITY STATEMENT
Approved for public release; distribution unlimited.

12b. DISTRIBUTION CODE

13. ABSTRACT (*Maximum 200 words*)

A previously developed transient aeroelastic rotor response analysis for shipboard engage/disengage sequences is utilized in the present research. The blade has elastic flap and torsion degrees of freedom and the equations of motion are discretized using the finite element method. The discretized equations of motion are integrated for a specified rotor speed run-upor run-down profile. Blade element theory is used to calculate quasi-steady or unsteady aerodynamic loads in linear and nonlinear regimes. Three deterministic wind gust distributions can be used to model the ship airwake environment. This analysis is modified to include a flap stop which restrains upper flap motion and a flap damper which damps flap hinge motion. In addition, an arbitrary gust model is incorporated into the analysis to enable more realistic airwake models. Validation studies are conducted using experimental data collected from a ship/helicopter model placed in a wind tunnel. Theoretical prediction show good agreement with experimewntal data for windward hub locations on the deck. A study of the effectiveness and feasiblility of a flap damper placed at the flap hinge is conducted. It indicates that a flap damper is an effective and feasible method to reduce downward tip deflections for an H-46 if the flap stop angle is raised. One study of the effects of pilot controllable parameters shows that the H-46 throttle advancement rate reduces the maximum downward tip deflections for spatially varying gusts.

14. SUBJECT TERMS
Sea Knight, Sea Stallion, MH-53E, HH-60H, Seahawk, CH-46D

15. NUMBER OF PAGES
19

16. PRICE CODE

17. SECURITY CLASSIFICATION OF REPORT	18. SECURITY CLASSIFICATION OF THIS PAGE	19. SECURITY CLASSIFICATION OF ABSTRACT	20. LIMITATION OF ABSTRACT
UNCLASSIFIED	UNCLASSIFIED	N/A	N/A

NSN 7540-01-280-5500

Standard Form 298 (Rev. 2-89)
Prescribed by ANSI Std. Z39-18

Enclosure (10)

VALIDATION AND APPLICATION OF A TRANSIENT AEROELASTIC ANALYSIS FOR SHIPBOARD ENGAGE/DISENGAGE OPERATIONS

William P. Geyer Jr.
Flight Test Engineer
Naval Air Warfare Center-Aircraft Division
Patuxent River, Maryland

Edward C. Smith
Assistant Professor of Aerospace Engineering
Pennsylvania State University
University Park, Pennsylvania

Jonathan Keller
Graduate Assistant
Pennsylvania State University
University Park, Pennsylvania

NOTATION

$\mathbf{C}$	Damping Matrix
C_{drag}	Aerodynamic drag constant
C_β	Rotational damping of flap damper
e_g	Chordwise offset of blade center-of-mass ahead of elastic axis
EI_{yy}	Flap bending stiffness
g	Acceleration due to gravity
GJ	Torsional Stiffness
h_{cg}	Vertical distance to hub with respect to ship coordinate system
$\hat{I}_I, \hat{J}_I, \hat{K}_I$	Unit vectors of inertial coordinate system
$\hat{I}_U, \hat{J}_U, \hat{K}_U$	Unit vectors of undeformed coordinate system
J	Rotor system rotational moment of inertia
k_m	Blade cross-sectional mass radius of gyration
K_β	Rotational spring stiffness of droop stop
$\mathbf{K}$	Stiffness Matrix
L	Blade section lift
m	Blade section mass
M	Blade section pitching moment
$\mathbf{M}$	Mass matrix
N	Number of finite beam elements
N_{dof}	Number of constrained degrees of freedom
$\mathbf{q}$	Global vector of nodal displacements
$\mathbf{Q}$	Load vector
R	Blade radius
t	Time
t_1	Initial time
t_2	Final time
T	Kinetic energy of the blade
T_{drag}	Torque on rotor system due to aerodynamic drag
u_F	Radial foreshortening term
U	Total potential energy
U_B	Potential (strain) energy of the blade
U_{DS}	Potential energy of the droop stop
U_{PL}	Potential energy of the pitch link
V_{roll}	Lateral wind component due to roll motion
V_{vert}	Vertical wind component in inertial coordinate system
V_{wod}	Relative wind-over-deck in inertial coordinate system
$\mathbf{V}_b$	Motion induced blade velocity vector for blade in undeformed frame
w	Blade displacement in z direction
w'_{DS}	Droop stop angle
W	Total work done
W_{AF}	Work done by the aerodynamic forces
W_G	Work done by gravitational forces
W_{NC}	Work done by flap damper forces
α_w	Angle wind vector above X_H-Y_H plane
$\delta(\,)$	Variation in ( )
$\Delta w'$	Rotation of flap hinge
$\Delta \dot{w}'$	Rotational velocity of flap hinge
ϕ	Elastic twist
ϕ_{max}	Maximum variation in ship roll angle
ϕ_S	Ship roll angle
Π	Total energy functional
θ_{75}	Collective pitch at 75% blade radius
ρ_s	Mass density
$\mathbf{T}$	Ship roll period
Ω	Rotor rotational speed

VALIDATION AND APPLICATION OF A TRANSIENT AEROELASTIC ANALYSIS FOR SHIPBOARD ENGAGE/DISENGAGE OPERATIONS

William P. Geyer Jr.
Flight Test Engineer
Naval Air Warfare Center-Aircraft Division
Patuxent River, Maryland

Edward C. Smith
Assistant Professor of Aerospace Engineering
Pennsylvania State University
University Park, Pennsylvania

Jonathan Keller
Graduate Assistant
Pennsylvania State University
University Park, Pennsylvania

NOTATION

$\mathbf{C}$	Damping Matrix
C_{drag}	Aerodynamic drag constant
C_β	Rotational damping of flap damper
e_g	Chordwise offset of blade center-of-mass ahead of elastic axis
EI_{yy}	Flap bending stiffness
g	Acceleration due to gravity
GJ	Torsional Stiffness
h_{cg}	Vertical distance to hub with respect to ship coordinate system
$\hat{I}_I, \hat{J}_I, \hat{K}_I$	Unit vectors of inertial coordinate system
$\hat{I}_U, \hat{J}_U, \hat{K}_U$	Unit vectors of undeformed coordinate system
J	Rotor system rotational moment of inertia
k_m	Blade cross-sectional mass radius of gyration
K_β	Rotational spring stiffness of droop stop
$\mathbf{K}$	Stiffness Matrix
L	Blade section lift
m	Blade section mass
M	Blade section pitching moment
$\mathbf{M}$	Mass matrix
N	Number of finite beam elements
N_{dof}	Number of constrained degrees of freedom
$\mathbf{q}$	Global vector of nodal displacements
$\mathbf{Q}$	Load vector
R	Blade radius
t	Time
t_1	Initial time
t_2	Final time
T	Kinetic energy of the blade
T_{drag}	Torque on rotor system due to aerodynamic drag
u_F	Radial foreshortening term
U	Total potential energy
U_B	Potential (strain) energy of the blade
U_{DS}	Potential energy of the droop stop
U_{PL}	Potential energy of the pitch link
V_{roll}	Lateral wind component due to roll motion
V_{vert}	Vertical wind component in inertial coordinate system
V_{wod}	Relative wind-over-deck in inertial coordinate system
$\mathbf{V}_b$	Motion induced blade velocity vector for blade in undeformed frame
w	Blade displacement in z direction
w'_{DS}	Droop stop angle
W	Total work done
W_{AF}	Work done by the aerodynamic forces
W_G	Work done by gravitational forces
W_{NC}	Work done by flap damper forces
α_w	Angle wind vector above X_H-Y_H plane
$\delta(\,)$	Variation in ( )
$\Delta w'$	Rotation of flap hinge
$\Delta \dot{w}'$	Rotational velocity of flap hinge
ϕ	Elastic twist
ϕ_{max}	Maximum variation in ship roll angle
ϕ_S	Ship roll angle
Π	Total energy functional
θ_{75}	Collective pitch at 75% blade radius
ρ_s	Mass density
T	Ship roll period
Ω	Rotor rotational speed

Encl (1)

Ω_0	Reference rotor rotational speed
ξ, η, ζ	Deformed coordinate system
ψ	Rotor blade azimuthal angle
ψ_{wod}	Relative wind-over-deck direction
$\bar{\psi}$	Nondimensional time

Subscripts and Superscripts

$()'$	$\partial(\,)/\partial x$
$\dot{()}$	$\partial(\,)/\partial t$
$\ddot{()}$	$\partial^2(\,)/\partial t^2$
$[\,]^T$	Transpose of vector or matrix
$()_a$	Inboard node of element
$()_b$	Outboard node of element
$()_i$	ith finite element
$()_m$	Center node of element
$()_U$	Value referenced to undeformed coordinate system

ABSTRACT

A previously developed transient aeroelastic rotor response analysis for shipboard engage/disengage sequences is utilized in the present research. The blade has elastic flap and torsion degrees of freedom and the equations of motion are discretized using the finite element method. The discretized equations of motion are integrated for a specified rotor speed run-up or run-down profile. Blade element theory is used to calculate quasi-steady or unsteady aerodynamic loads in linear and nonlinear regimes. Three deterministic wind gust distributions can be used to model the ship airwake environment. This analysis is modified to include a flap stop which restrains upper flap motion and a flap damper which damps flap hinge motion. In addition, an arbitrary gust model is incorporated into the analysis to enable more realistic airwake models. Validation studies are conducted using experimental data collected from a ship/helicopter model placed in a wind tunnel. Theoretical prediction show good agreement with experimental data for windward hub locations on the deck. A study of the effectiveness and feasibility of a flap damper placed at the flap hinge is conducted. It indicates that a flap damper is an effective and feasible method to reduce downward tip deflections for an H-46 if the flap stop angle is raised. One study of the effects of pilot controllable parameters shows that the H-46 throttle advancement rate reduces the maximum downward tip deflections for spatially varying gusts.

INTRODUCTION

Navy helicopters provide some of the most crucial defense measures for the carrier battle groups. The Sea Stallion (MH-53E) sweeps waters ahead of the carrier battle group for mines while the Seahawk (SH-60B) scouts for enemy submarines. Other important roles are rescue operations conducted by the Seahawk (HH-60H) and vertical replenishment conducted by the Sea Knight (CH-46D). While on deployment, these tasks must be carried out even in the most adverse weather. However, ship motion and highly turbulent airwake over the flight deck increase the difficulty of maintaining high tempo of flight operations. For most aircraft, the dynamic interface challenge begins during the launch and ends with the recovery, but for the H-46, this challenge begins with rotor engagement and ends with rotor disengagement.

During rotor engage and disengage, the blade passes through low rotor speed regions where aerodynamic forces are large compared to centrifugal stiffening effects. In some conditions, the aeroelastic flapping of the blades becomes large enough for the rotor blades to contact the fuselage. The H-46 community terms this a "tunnel strike" and is depicted in Figure 1. Blade/fuselage contact occurs mostly in high wind and sea state conditions and has plagued the Sea Knight since it became operational in 1964. Extensive experimental testing is required to ensure safe engage/disengage evolutions.

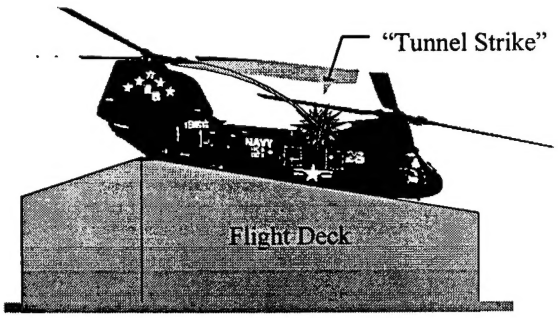

Figure 1: Depiction of a tunnel strike.

The Naval Air Warfare Center Aircraft Division, located in Patuxent River Maryland, conducts all H-46 engage/disengage testing. The goal of this testing is to provide the fleet safe H-46 engage/disengage envelopes. A sample envelope is shown in Figure 2. The shaded area indicates to pilots and ship's personnel the relative wind-over-deck conditions that are conducive to safe engage/disengage evolutions.

Five experimental H-46 engage/disengage tests conducted between 1974 and 1987 are reported in Refs. 1-5. All provided blade to fuselage clearance

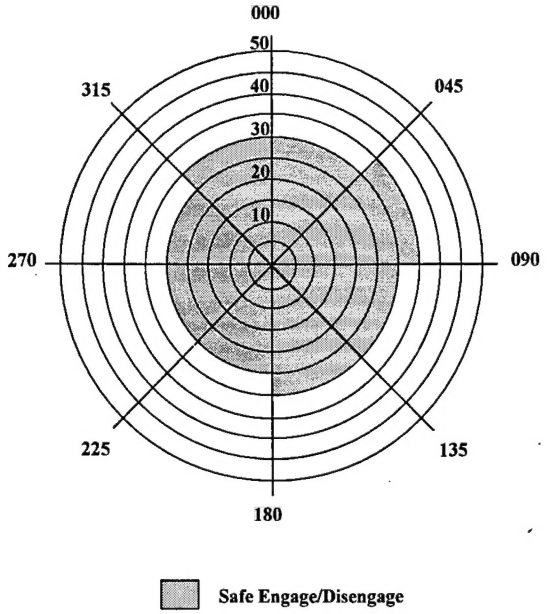

Figure 2: Sample engage/disengage envelope.

data for ship classes certified for H-46 flight operations. The paragraphs that follow summarize the qualitative comments on blade behavior and pilot procedures described in these reports.

Several pilot procedures were incorporated to reduce the chances of a tunnel strike. The speed trim setting (which added longitudinal cyclic pitch to tilt the rotor disk) was changed from "taxi" to "auto" which was found to provide more blade tip-to-fuselage clearance [1]. In addition, pilots were cautioned not to engage if pre-engagement blade flapping was more than one foot at the tips [2,3].

Engineers made several qualitative comments on contributing factors to the tunnel strike phenomenon. Hurley et al. [4] explains that the excessive flapping was believed to be due solely to the horizontal and vertical wind components [4]. While another observation states that ship motion and turbulence also contributed to this excessive flapping phenomenon [5]. A test observation also noted that blade behavior was dependent upon the aircraft position relative to the deck edge. The portion of the rotor arc that extended over the flight deck edge was observed to be affected by the airflow more than if the entire rotor disk was over the flight deck [4,5].

Since 1985, Newman has been conducting a systematic study focused on analytically modeling the transient flap dynamics during engage/disengage sequences, typically referred to as "blade sailing" in the United Kingdom. Initially, a flapwise elastic model of a semi-rigid rotor system was developed which employed a nonlinear quasi-steady aerodynamics model [6]. Rotor speed run-up and run-down time histories were predicted using basic rotor system dynamic and blade aerodynamic laws. The ship airwake environment was modeled by a simple deterministic gust and ship roll motion effects on wind. The deterministic gust was developed from limited full-scale and wind tunnel ship airwake data. Newman [7] later improved this model by including flap-torsion coupling in the aerodynamics and modifying the existing deterministic gust model based on extensive model scale ship airwake studies.

In 1992, Newman [8] modified the elastic flap code to model articulated (hinged) rotor systems. For this type of rotor, the blade motion at low rotor speeds was constrained to both upper and lower limits using mechanical flap and droop stops. These stops were modeled by using conditional point springs that apply a restraining force a small distance from the flap hinge. Tip deflections for the articulated rotor were shown to be much larger than those for the semi-rigid rotor.

Efforts to validate the flapwise elastic rotor code included comparison to full-scale data and model scale wind tunnel data. The full-scale data was collected using an Aerospatiale SA330 Puma helicopter for rotor run-up and run-down in a 10 knot headwind [9]. The comparison was conducted for flapping motion only. Characteristics of the Puma blade flap motion were shown to be reproduced; however, some rotor speed data at low speeds was lost and was interpolated. The flapping responses at operating rotor speed were in good agreement, but coning angles differed by 1 degree at the blade cuff.

Newman [9] further validated the theoretical model under more controlled conditions using a wind tunnel model. A helicopter wind tunnel model was constructed from a radio control model which was instrumented to measure flap angle, pitch angle, rotational speed, and blade position. Flap angle and pitch angle were measured using potentiometers. Blade position and azimuth were measured using a transducer. The helicopter model was mounted on a scaled flight deck and subjected to beam winds approaching from the port direction. It was found that the largest flap deflections occurred for the hub located a quarter of the deck's width from the windward edge. The mildest flap deflections occurred for the hub located one quarter of the deck's width from the leeward edge; therefore, the influence of the ship's structure is very important to the blade behavior.

The authors of this work developed a transient aeroelastic rotor response analysis for shipboard

engage/disengage sequences [10]. The blade was modeled as an elastic beam undergoing deflections in flap bending and torsion. The finite element method was used to spatially discretize the nonuniform blade governing equations. This analysis models both hingeless and articulated rotor systems including droop stops that limit flap hinge motion during low rotor speeds for articulated rotors. The discretized blade equations of motion are integrated in modal space for a specified rotor speed run-up or run-down profile. Blade element theory was used to calculate quasi-steady or unsteady aerodynamic loads in linear and nonlinear regimes. Three different simple wind gust distributions were modeled. Basic ship roll motion characteristics were also included in the shipboard airwake environment. An H-46 rotor system model was developed and showed excellent correlation with static tip deflection and blade natural frequency data. Using this analysis, the blade was shown to demonstrate response characteristics that were dependent upon the type of deterministic gust; higher levels of structural and aerodynamic fidelity were suggested for spatially varying deterministic gust; and control inputs were shown to have a moderate effect on maximum downward tip deflection.

The present research is focused on validating the transient rotor response against wind tunnel model data collected reported in Ref. 9. Other efforts are concentrated on applying this analysis to reduce the risk of a tunnel strike. Pilot controllable parameters including rotor system acceleration, pitch control settings, and blade start azimuth are studied to determine their effect on maximum downward tip deflections. In addition, the feasibility and effectiveness of incorporating flap damping at the blade root is investigated.

HELICOPTER MODEL FORMULATION

This analysis predicts the transient aeroelastic response for a single blade of a helicopter with an articulated or hingeless rotor system. The helicopter is resting on the flight deck of a ship with the aircraft's longitudinal axis aligned with the ship's longitudinal axis. Simple deterministic and arbitrary gusts developed in Refs. 6-9 are employed to model the shipboard aerodynamic environment. Ship roll motion is also included in the aerodynamic environment. Contributions of ship roll motion to the blade inertia forces are neglected in the structural model because ship motion frequencies relative to the rotor frequency are small [7]. Gravity is included in this transient model because gravitational forces relative to centrifugal forces are significant in low rotor speed regions and at rest. The following section briefly describes the analysis. A more detailed description is presented in Ref. 10.

Blade flap (i.e. transverse out-of-plane bending), w, and torsional deflections, ϕ, are referenced to a plane perpendicular to the shaft axis. The equations that govern the flap and torsion motions of the nonconservative, aeroelastic system are derived using the generalized Hamilton's Principle (Eqn. 1).

$$\delta\Pi = \int_{t_1}^{t_2} (\delta T - \delta U + \delta W)dt = 0 \qquad (1)$$

where δT is the variation of kinetic energy, δU is the variation of strain energy, and δW is the virtual work due to external forces.

KINETIC ENERGY

The blade kinetic energy is the energy of the blade due to its velocity. Therefore the kinetic energy terms capture the inertial effects of blade motion. Recall that inertial effects due to ship motion are considered negligible. An inertial effect due to rotational blade motion is centrifugal stiffening. A radial foreshortening term, u_F, is used to account for the centrifugal stiffening effects on flap motion and is defined as

$$u_F = \int_0^x w'\delta w' d\xi \qquad (2)$$

A more detailed explanation of this term's origin is found in Ref. 11. The variation of kinetic energy is expressed as

$$\delta T = \int_0^R \iint_A \rho_s \mathbf{V}_b \cdot \delta\mathbf{V}_b \, d\eta \, d\zeta \, dx \qquad (3)$$

where ρ_s is the mass density and $\mathbf{V}_b$ is the blade velocity relative to the hub.

STRAIN ENERGY

The variation of strain energy can be expressed as a summation of different contributions

$$\delta U = \delta U_B + \delta U_{DS} + \delta U_{PL} \qquad (4)$$

where δU_B is the variation of blade strain energy, δU_{DS} is the variation of droop stop strain energy, and δU_{PL} is the variation of pitch link strain energy.

Blade Strain Energy

Blade strain energy is the potential energy stored in the blade due to deformations. The flap and torsion deflections are predicted using Bernoulli-Euler beam bending theory. Based upon the assumptions of this theory, the blade is a long slender beam that undergoes small strains but can have moderate deflections. Assuming isotropic elastic

properties, the variation of blade strain energy can be expressed as

$$\delta U_B = \int_0^R \iint_A (E\varepsilon_{xx}\delta\varepsilon_{xx} + G\varepsilon_{x\eta}\delta\varepsilon_{x\eta} + G\varepsilon_{x\zeta}\delta\varepsilon_{x\zeta})d\eta d\zeta dx \quad (5)$$

where ε_{xx} is the axial strain, $\varepsilon_{x\eta}$ and $\varepsilon_{x\zeta}$ are engineering shear strains, E is the axial modulus of elasticity, and G is the shear modulus of elasticity.

Droop and Flap Stops

The droop stop is a passive mechanism, illustrated in Figure 3, that is extended and retracted by centrifugal force acting on a counterweight. During low rotor speeds and at rest, this mechanism restrains the flap hinge from rotating below a certain angle, termed the droop stop angle. At a particular rotor speed, the droop stop will retract during rotor engagement and extend during rotor disengagement. In addition, two situations must be modeled to ensure proper physical behavior of the droop stop. During rotor engagement, the blade may be in contact with the droop stop upon reaching the rotor speed at which the droop stop can retract. The droop stop cannot retract until the blade lifts off of the droop stop. During rotor disengagement, the hinge angle may be below the droop stop angle upon reaching the rotor speed at which the droop stop can extend. The hinge angle must be above the droop stop angle to enable the droop stop to extend.

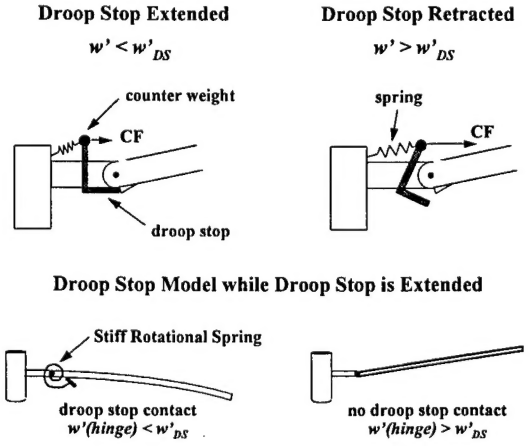

Figure 3: Droop stop physics and how it is modeled.

The description given above on droop stop physics shows that the droop stop status (extended/retracted) depends on flap hinge angle and rotor speed. This analysis models the droop stop interaction with the blade using a conditional rotational spring located at the flap hinge (see Figure 3). While the droop stop is extended, the rotational spring stiffness is zero for hinge angles greater than the droop stop angle and very large for hinge angles below the droop stop angle. The variation of strain energy due to the droop stop is expressed as

$$\delta U_{DS} = K_\beta(\Delta w' - w'_{DS})\delta\Delta w' \quad (6)$$

where K_β is the rotational spring stiffness, $\Delta w'$ is the blade rotation at the flap hinge, and w'_{DS}, droop stop angle, is the specified hinge angle for droop stop contact.

The flap stop restrains upward flap motion during low rotor speeds in the same manner as the droop stop. The flap stop contact angle and rotor speed for flap stop extension and retraction is independent of the droop stop counterparts. The formulation used for flap stops is similar to the droop stop.

VIRTUAL WORK

The virtual work can be expressed as a summation of different contributions similar to the variation of strain energy

$$\delta W = \delta W_G + \delta W_{NC} + \delta W_{AF} \quad (7)$$

where δW_G is the virtual work due to gravity forces, δW_{NC} is the virtual work due to the flap damper, and δW_{AF} is the virtual work due to the aerodynamic forces.

Gravitational Force

As stated earlier, gravitational forces are required in this analysis due to their effect on blade deflection over the low rotor speed regions. The work performed on the blade due to gravitational forces is expressed as

$$W_G = -\int_0^R mg\hat{K}_I \cdot w\hat{K}_U dx \quad (8)$$

where g is the acceleration due to gravity (assumed downward acceleration positive). This analysis assumes that the ship motion effects on inertia and the shaft tilt angles are small; therefore, the nondimensional virtual work is expressed as

$$\delta W_G = -\int_0^1 mg\delta w dx \quad (9)$$

Flap Damping

The effect of a rotational damper acting at the flap hinge on the blade deflection was investigated in this analysis. The virtual work performed on the blade due to the flap damper is expressed as

$$\delta W_{NC} = -C_\beta \Delta\dot{w}'\delta\Delta\dot{w}' \quad (10)$$

where C_β is the rotational flap damping and $\Delta\dot{w}'$ is the blade angular velocity at the flap hinge. The flap damper was assumed to extend/retract at the same

rotor speed as the droop and flap stops; however, unlike the droop and flap stops, the flap damper was engaged regardless of the flap hinge angle.

Airloads

The shipboard aerodynamic environment is characterized by a very complex flowfield. The ship's superstructure causes highly non-uniform flow over the flight deck and ship motion can increase inflow through the rotor disk; therefore, accurate models of the shipboard aerodynamic environment and the blade element aerodynamics are equally important. The effect of these models on the equations of motion is represented in the virtual work term. The virtual work performed by the aerodynamic forces in the undeformed frame is expressed as

$$\delta W_{AF} = \int_0^1 \left[(L)_U \delta w + (M)_U \delta \phi \right] dx \qquad (11)$$

where $(L)_U$ and $(M)_U$ are the normal force and pitching moment about the quarter chord. The next two sections briefly describe the shipboard aerodynamic environment model and blade element aerodynamic theories employed in this analysis.

SHIPBOARD AERODYNAMIC ENVIRONMENT

The shipboard aerodynamic environment has been simplified to increase computational efficiency but more importantly to distinguish the effects of certain airwake characteristics on the blade response. The ship is assumed to be stationary with respect to the inertial coordinate system except for roll motion. The atmospheric winds relative to the ship are uniform. These winds are termed the relative Wind-Over-Deck (WOD) conditions. They are defined in the inertial reference frame by a wind speed, V_{wod}, and direction, ψ_{wod}, and a vertical wind component, V_{vert}. The relative WOD speed and direction describes the wind speed and the direction from which the wind approaches the ship and a zero WOD direction describes winds that approach the bow of the ship. Simple and arbitrary deterministic gust models are used to model local variations over the rotor disk due to ship airwake non-uniform characteristics.

NAWCAD Pax River limits launch and recovery operations for only pitch and roll ship motions. In addition, pitch and roll are suggested in Ref. 12 to be the dominant ship motions. Only roll motion is used in this analysis to remain consistent with Refs. 7-9. The ship roll motion aerodynamic model consists of the transformed relative WOD conditions due to the ship roll angle and a wind component at the hub height due to the angular roll velocity (shown in

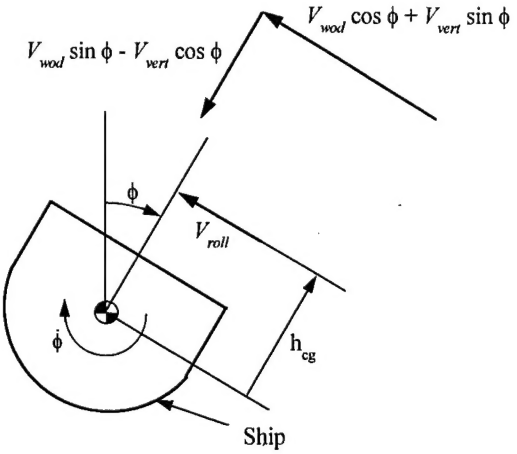

Figure 4: Ship motion effects on wind velocities in the ship coordinate system.

Figure 4). Ship roll motion is governed by sinusoidal variation of the roll angle, ϕ_S. The lateral velocity, V_{roll}, at the hub height due to roll angular velocity is expressed as

$$V_{roll} = \phi_{max} h_{cg} \left(\frac{2\pi}{T} \right) \cos\left(\frac{2\pi\bar{\psi}}{T} \right) \qquad (12)$$

where ϕ_{max} is the maximum roll angle, h_{cg} is the vertical distance in the ship reference frame from the ship's center of gravity to the aircraft hub, and T is the nondimensional ship roll period.

Ship airwake was shown to be turbulent and spatially dependent in airwake studies conducted in Ref. 7. Two gust models that simulated the air flow over a ship flight deck subjected to a crosswind were a result of these studies. The step and linear gust models are shown in Figure 5. These models are adopted in this analysis to explore the effects of local wind variations over the disk on the blade response. The deterministic gusts consist of an upward wind component on the windward half of the rotor disk, a downward wind component on the leeward half of the disk, and a lateral wind component in the direction of the relative WOD velocity. The magnitude of these components are specified as fractions of the relative WOD velocity. In addition a simple uniform inflow gust is included in this analysis where α_w is the angle of the uniform gust with respect to the horizon..

BLADE ELEMENT AERODYNAMICS

The quasi-steady aerodynamics development follows a similar unsteady thin airfoil theory development by Johnson [13]. In the unsteady thin airfoil development, the airfoil is modeled by two

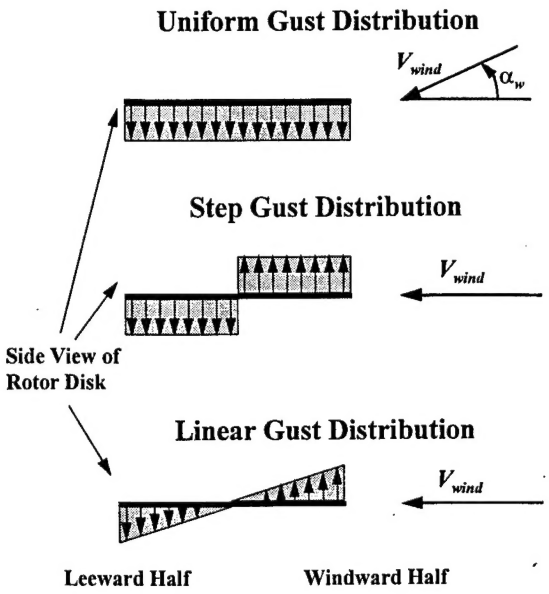

Figure 5: Deterministic gust distributions.

thin vortex sheets, one being the airfoil and the other a shed wake. Since this is a quasi-static development, the unsteady deficiency function is neglected. This development also includes the airloads due to virtual mass (noncirculatory) effects. The analysis can predict both linear and nonlinear airloads where nonlinear airloads are calculated using Kirchhoff's nonlinear separation model.

The unsteady aerodynamic model used in this analysis was developed by Leishman and Beddoes. Significant documentation on the development of this model can be found in Refs. 14-17. This time domain model has three levels of fidelity, attached flow unsteady aerodynamics, nonlinear aerodynamics, and dynamic stall. The attached flow unsteady model is based on an indicial response formulation and predicts both noncirculatory and circulatory airloads. The nonlinear aerodynamics model accounts for trailing edge separation, leading edge pressure lags, and unsteady boundary layer effects. Lastly, the dynamic stall portion of the unsteady aerodynamic model calculates the additional lift and large downward pitching moment created by the shedding vortex.

A detailed description of the formulation of the quasi-steady airloads and incorporation of Leishman and Beddoes' unsteady aerodynamic model into the present analysis given in Ref. 10.

DISCRETIZED BLADE EQUATIONS OF MOTION

The generalized Hamilton's principle, Eqn. (1), is being used to formulate the blade equations of motion. The finite element method is used to formulate the discretized blade equations of motion. The nondimensional virtual energy expression for the discretized blade can be written as

$$\delta\Pi = \int_{\bar{\psi}_1}^{\bar{\psi}_2} \left[\sum_{i=1}^{N} (\delta T_i - \delta U_i + \delta W_i) \right] d\bar{\psi} \qquad (13)$$

where i is the *ith* beam element and N is the total number of beam elements in blade.

An illustration of the blade finite element discretization is shown in Figure 6. Each of the N flexible elements has three nodes, two external and one internal, which describe the elemental displacements. Each external node has w, w', and ϕ nodal displacements and the internal node only has a ϕ nodal displacement; therefore, each element has seven degrees of freedom (w_a, w'_a, ϕ_a, ϕ_m, w_b, w'_b, and ϕ_b). The deformations along the element are interpolated from the nodal displacements using shape functions which are derived from a cubic Hermitian polynomial for flap deformation and a quadratic Lagrangian polynomial for torsion deformation.

The energy expressions are spatially discretized by substituting the shape functions into the elemental virtual energy expressions. The resulting expressions are integrated in space using a six point Gaussian Quadrature method. The virtual energy expression in terms of the elemental matrices and load vector becomes

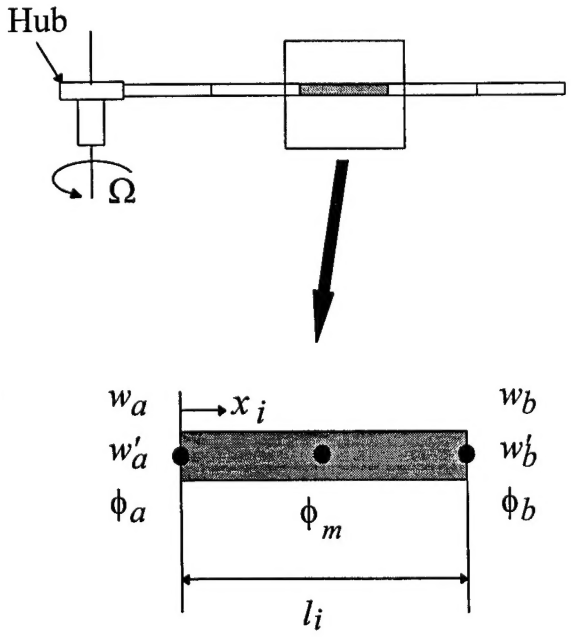

Figure 6: Blade elemental degrees of freedom.

$$\delta\Pi = \int_{\bar{\psi}_1}^{\bar{\psi}_2} \left[\sum_{i=1}^{N} \delta \mathbf{q}_i^T (\mathbf{M}_i \ddot{\mathbf{q}}_i + \mathbf{C}_i \dot{\mathbf{q}}_i + \mathbf{K}_i \mathbf{q}_i - \mathbf{Q}_i) \right] d\bar{\psi} \quad (14)$$

where $\mathbf{M}_i$, $\mathbf{C}_i$, and $\mathbf{K}_i$, are the elemental mass, damping and stiffness matrices, respectively, and $\mathbf{Q}_i$ is the elemental load vector. The airloads are divided into motion dependent and independent terms. All motion dependent quasi-steady terms are combined with the corresponding elemental mass, stiffness, or damping matrix. All unsteady and motion independent quasi-steady terms are combined with the elemental load vector.

The assembly process provides flexibility in modeling different types of rotor systems including both hingeless and articulated. Once the global mass, damping and stiffness matrices and load vector are assembled, the global virtual displacements, $\delta\mathbf{q}$, are arbitrary and the discretized equations of motion become

$$\mathbf{M}\ddot{\mathbf{q}} + \mathbf{C}\dot{\mathbf{q}} + \mathbf{K}\mathbf{q} = \mathbf{Q} \quad (15)$$

Lastly, kinematic boundary conditions are applied to the global matrices and load vector by setting the degree of freedom that corresponds to boundary condition equal to zero.

ANALYSIS

The discretized equations of motion can be used to perform three analyses; eigenanalysis, transient response analysis, and engage/disengage envelope analysis. These analyses are interdependent because the eigenanalysis is required for the transient response analysis and the transient response analysis is used in the engage/disengage envelope analysis. The sections that follow will briefly describe the transient response and engage/disengage envelope analyses.

Transient Response Analysis

The blade transient response is calculated by integrating the discretized blade equations of motion for a specified rotor speed run-up/run-down profile. The integration is performed using a 4th order Runge-Kutta scheme. The blade static deflection is used as the initial conditions for rotor run-up solution. The steady state response at the operational rotor speed is used as initial conditions for run-down solutions.

The blade response can be computed in either physical or modal space but integration in modal space provides greater computational efficiency. The process called modal analysis reduces an N_{dof} system to N_{dof} independent single degree of freedom systems. Each independent single degree of freedom system corresponds to a blade structural mode of vibration. This simplification provides great insight into the contribution of each structural mode to the blade response. Unfortunately, motion dependent aerodynamic loads complicate this simplistic representation. The damping and stiffness matrices are typically not symmetric and the resulting modal system is no longer an uncoupled set of differential equations. The computational power of the integration in modal space comes from the ability to approximate the blade motion using the first few modes of vibration. The higher modes provide little contribution to the blade response.

Recall that a very stiff rotational spring is used to freeze the hinge during blade/droop stop contact. Once the blade lifts off the droop stop, the rotational spring is removed from the system. Blade deflection during droop stop contact is due purely to elastic deformation with no rigid body rotation at the hinge. In both physical and modal space, the integration scheme requires smaller time steps to approximate the blade response due to discontinuities in rotational spring stiffness. In addition, the normal modes used to compute this motion in modal space do not represent purely elastic deformation and require more flap modes to approximate the blade shape. Details of this study are presented in Ref. 10.

The modal swapping technique is developed to circumvent the integration problem in modal space. Before integration begins, an eigensolution is found for the structure with and without the droop stop rotational spring included for Ω/Ω_0=1. During integration, the modal vector without the rotational spring effects is used to transform the system into modal space while there is no blade/droop stop contact; however, when contact occurs, the modal vector with rotational spring effects is used to transform the system into modal space.

Engage/Disengage Envelope Analysis

The engage/disengage (E/D) wind envelope is a graphical tool used to determine the wind conditions for safe E/D sequences. An example of an E/D wind envelope was given in Figure 2 where the shaded area depicts the wind conditions that provide safe E/D sequences. This analysis tool uses the blade transient response to calculate the maximum negative tip deflection for an E/D sequence. This section describes how this data is manipulated to develop these envelopes.

This analysis provides wind envelope results in tabular form for either an engage or disengage event. The manipulation of blade transient response is the same for both events. The program is set up to

Table 1: Blade clearance scale criteria.

BCS Rating	Blade/Fuselage Clearance (inches)
1	> 23
2	8 - 23
3	0 - 8
4	Blade/Fuselage Contact

provide maximum negative tip deflections for 240 wind conditions where wind azimuth is varied every 15 degrees and wind speed is varied every 5 knots. The data from the engage or disengage events is rated according to a blade clearance scale (BCS). The blade clearance scale criteria is given in Table 1. When a blade from the aft rotor hub of the H-46 is positioned above the synchronization shaft, the tip deflection required to strike the synchronization shaft cover is 55 inches. This tip deflection and the BCS criteria are used to determine tip deflections necessary for each blade clearance rating and further analysis is conducted to define boundaries of different blade clearance ratings.

This analysis tool is designed to automate wind envelope production; therefore, the boundaries of each rating must be defined. A simple example is used to clarify the process used to define rating boundaries. Figure 7 is a sample wind envelope plot with blade clearance rating results overlaid. Wind conditions for safe E/D sequences are denoted by ratings lower than three; therefore, the BCS 2 boundary determines the safe region. Note that from wind condition 090/20 (wind direction/wind speed) to wind condition 090/25 the rating jumps from a one to a four. The BCS 2 boundary is located at the lower rating to provide a conservative envelope.

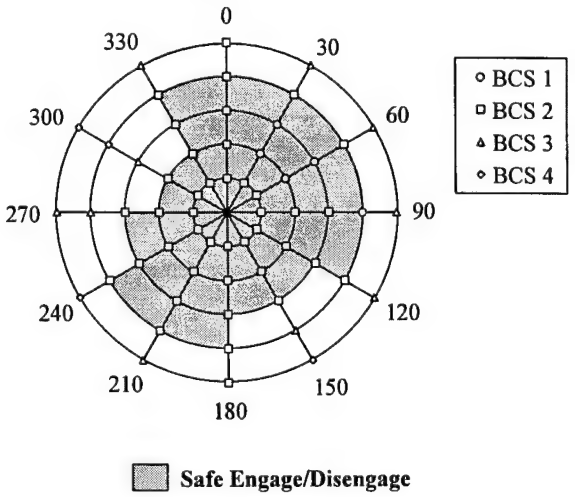

Figure 7: Generic engage/disengage wind envelope with blade clearance scale ratings overlaid.

VALIDATION

As stated earlier, Ref. 9 conducted a wind tunnel experiment on a model scale rotor system and results of this study were used to validate the theoretical model. The present research uses the results of this wind tunnel experiment to validate the transient dynamic response predicted by the aeroelastic analysis. Initially, this section discusses the wind tunnel model and airwake measurements presented in Ref. 9. Next, modifications to the aeroelastic analysis, including the arbitrary gust model, and the rotor system model are discussed. Finally a comparison of theoretical and experimental results is discussed.

WIND TUNNEL EXPERIMENT

A radio control model was chosen to represent the height to rotor diameter ratio of the Westland Lynx; however, most models had stiff blades and teetering rotor systems unlike the semi-rigid rotor system of the Lynx. Several modifications had to be made to incorporate the radio control model into the wind tunnel experiment. First, the powerplant, a 10cc gas powered engine, was not suitable due to exhaust fumes and vibration; therefore, an electric engine from a spin dryer was used instead. The engine was mounted under the simulated flight deck and circuitry was added to control the engine speed. Second, measurement devices were mounted to the rotor system to record rotor speed, rotor azimuth, blade teetering angle, and blade pitch. Rotor speed and azimuth were recorded by an optical modular shaft encoder attached to the rotor shaft extension. Blade teetering angle and blade pitch were recorded by linear potentiometers. Lastly, one blade was removed and replaced by a counterbalance to isolate the aerodynamics of a single rotor blade.

The helicopter model was mounted on a scale version of a Rover Class Royal Fleet Auxiliary flight deck. The flight deck consisted of a wooden box sized to match the scale of the helicopter model. The ship/helicopter combination was mounted in the wind tunnel to represent the ship in port beam winds with the helicopter aligned along the longitudinal axis of the ship. The helicopter was mounted on a sliding rail to easily move it to 5 positions laterally on the simulated flight deck.

Airwake measurements were taken to provide data for the theoretical model. The wind tunnel was run at speeds of 2.5 and 5 m/s to simulate full-scale wind speeds. A laser doppler anemometer was used

to measure the airwake. Results of this test are shown in Figures 8 and 9. For each rotor hub location winds were measured along the direction of wind flow. The variation over the rotor disk is shown for each hub location in Figure 8. Note that the three upwind hub locations show a point where wind speed drops off and the last two locations show an overall decrease in wind speed. These results demonstrate a very distinct division between laminar and turbulent flow regions. Figure 9 illustrates the variation of flow inclination over the rotor disk for the five hub locations. Note the large change in flow inclination for the three leeward hub locations which is indicative of reverse flow.

THEORETICAL MODEL

The present analysis was modified to conduct the validation. This analysis only models hingeless and articulated rotor systems; therefore, only single blade experiments were used in the comparison and a counterbalance was added. In addition, the analysis

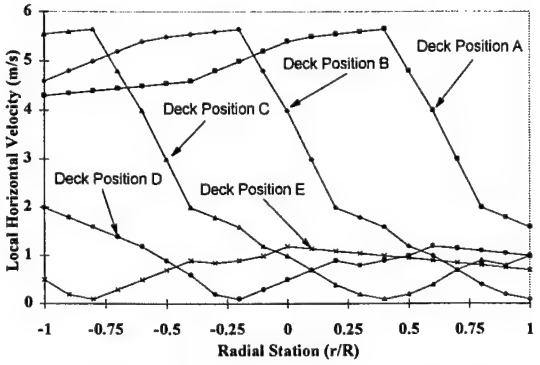

Figure 8: Variation of local horizontal flow velocity over the rotor disk for five hub locations.

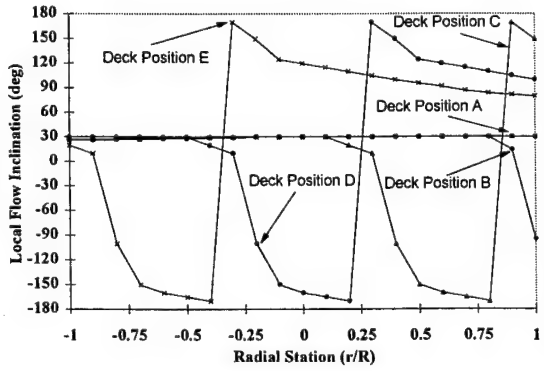

Figure 9: Local flow inclination over the rotor disk for five hub locations.

was modified for an arbitrary gust. The components of velocity in the direction of freestream wind and vertically are arbitrary while the lateral component is assumed to be zero. The arbitrary velocity components only vary over the centerline of the rotor disk in the direction of the freestream wind velocity. Arbitrary velocity components for points on the rotor disk perpendicular to the freestream flow are the same as the corresponding centerline values. Averaged values of the velocity components presented in Ref. 9 are used in this validation. A linear interpolation method is used to determine values of velocity components at points not collected in the wind tunnel experiments.

A model was developed to represent the aerodynamic and structural qualities of the radio control model. The rotor system was modeled using a teetering flexurally stiff blade. Rigid flap and droop stops restrained flap motion at 23 and -11 degrees, respectively. The root cutout was modeled at 14% and a NACA 0012 airfoil was employed. A collective setting of zero degrees was used to provide no thrust and a cyclic setting of 1.4 degrees was suggested by Ref. 9 to account for unforeseen cyclic input. It was difficult to judge the initial conditions of the results presented in Ref. 9; therefore the rotor speed profiles followed the theoretical ones presented

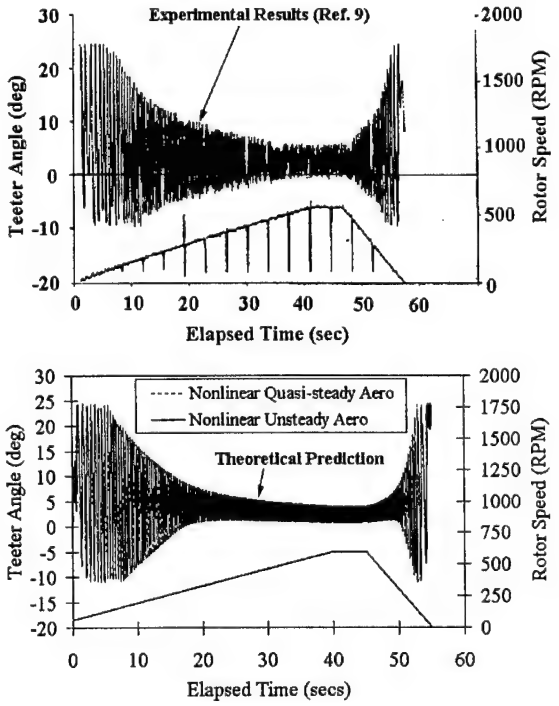

Figure 10: Comparison of experiment and theoretical blade response for deck position A.

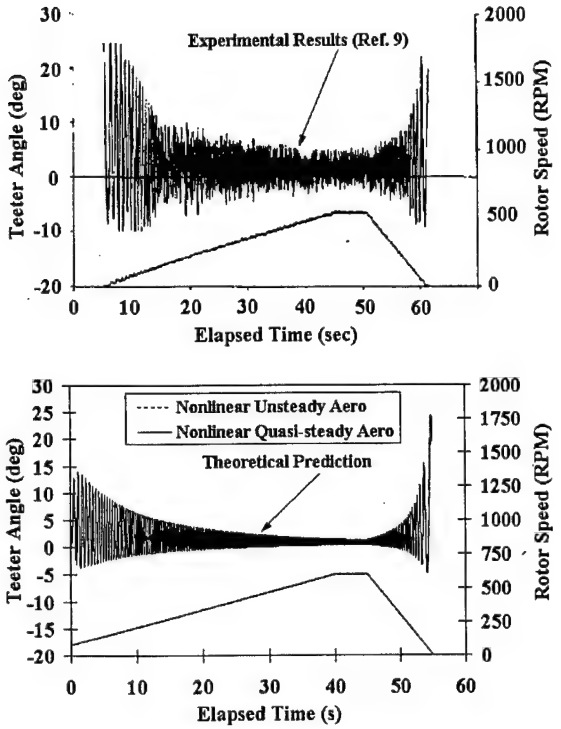

Figure 11: Comparison of experimental and theoretical blade response for deck position C.

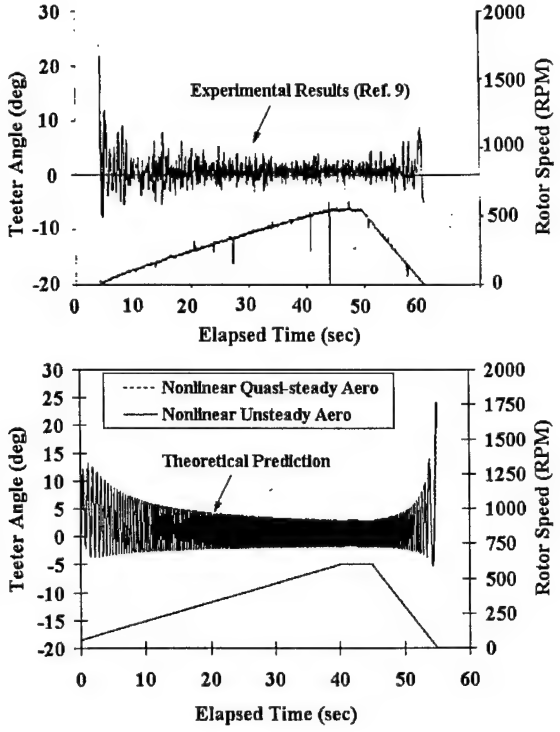

Figure 12: Comparison of experimental and theoretical blade response for deck position E.

in Ref. 9 and the blade was started pointing into the wind.

COMPARISON OF RESULTS

The analysis was compared to the experimental data for each hub location and both cyclic settings. All results shown are for rotor run-up. For each figure, the experimental response is shown on top and the theoretical predictions are shown on bottom. Figure 10 shows the comparison for deck position A. In general, note that the experimental data shows very little random behavior as might be expected in a laminar airwake. In this case, the theoretical predictions show good agreement with experimental results. The responses for deck position C are shown in Figure 11. Note the experimental results show more random behavior which is expected since more of the rotor is emersed in turbulent flow. The theoretical results still show good agreement with overall trends of the experimental data. Lastly, note the difference in behavior when the rotor is fully emersed in the turbulent airwake (deck position E), seen in the random blade response, as shown in Figure 12. Note that the theoretical results do not agree very well with experimental data since the temporal airwake variations are not modeled.

In Figures 10-12, theoretical results were shown for quasi-steady and unsteady nonlinear aerodynamics. Note that the unsteady aerodynamics is shown to be more important for deck position A than for deck positions C and E. Figure 13 provides a closer examination of the theoretical predictions for deck position A. Note that the hinge angle response produced using unsteady aerodynamics shows increased downward tip deflections in the first 3 seconds which suggests dynamic stall. In addition, note the phase lag in the hinge angle results for the unsteady aerodynamics. The increased damping provided by the unsteady aerodynamics is also shown in the time histories of the separation parameters. Note that the blade does not experience stall regions at a lower rotor speed for unsteady aerodynamics. This illustrates the importance of a higher fidelity aerodynamic model for large velocity changes in spatially varying flows.

ENGAGE/DISENGAGE ANALYSIS

In the previous sections, the helicopter model formulation was briefly described emphasizing the droop and flap stops model and the engage/disengage envelope analysis. Also the transient response analysis was validated against experimental data collected from a model scale rotor system. Initially,

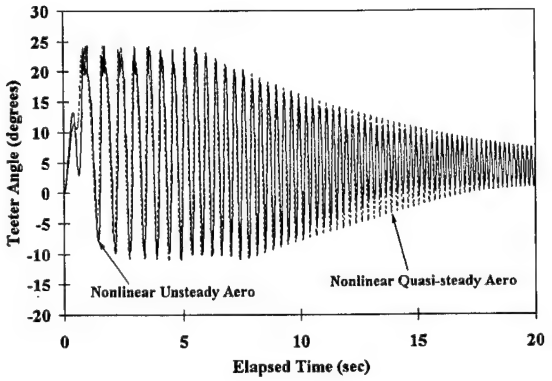

Figure 13: A comparison of blade response for two aerodynamic models at deck position A.

this section discusses the effectiveness and feasibility of incorporating flap damping to reduce the risk of tunnel strikes. Other studies investigate the effects of pilot controllable parameters, such as control inputs, blade start azimuth, and rotor speed run-up/run-down profile variations, on transient blade response.

This research is focused on the tunnel strike phenomenon of the H-46 Sea Knight which is a medium lift, tandem rotor aircraft employed by the U.S. Navy and U.S. Marines. The operational rotor speed of both rotor systems is 264 RPM. The engagement rotor speed profile developed from limited experimental data is shown in Figure 14. Each blade is 25.5 feet in length from shaft to tip and has a chord of 1.5625 feet. The actual variations of EI_{yy}, GJ, m, mk_m^2, and e_g with radial station are modeled using 12 finite elements. The structural properties and the finite element representation are presented in Ref. 10. The flap hinge is located 5 inches outboard of the shaft and the droop and flap stop angles are -0.54 and 1.5 degrees, respectively. The blade is linearly twisted -8.5 degrees from the shaft to the tip (nose down at the tip). The NACA 0012 which is not the actual H-46 airfoil is employed

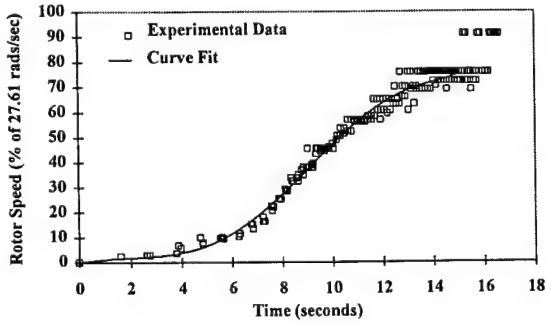

Figure 14: H-46 run-up rotor speed profile developed from limited experimental data.

in this model due to the large amounts of data available on its unsteady aerodynamics, nonlinear separation and dynamic stall characteristics.

The present research only models the aft rotor system of the H-46. The shaft of the aft rotor system is tilted forward 2.58 degrees with respect to the ship coordinate system. During all rotor engage/ disengage sequences, the collective, θ_{75}, is set at 3 degrees and the "auto" cyclic trim setting is selected. The "auto" cyclic trim setting tilts the aft rotor disk 2.5 degrees aft from a plane perpendicular to the shaft axis for a no wind condition. The cyclic control inputs required to obtain this blade response are determined from rigid blade flap dynamics. Assuming negligible inflow and no wind, the longitudinal and lateral cyclic control inputs are 2.5 degrees and 0.0693 degrees, respectively. These control inputs are termed the standard control inputs for the present research and are used to produce all results unless otherwise noted.

The two baseline aerodynamic environments used in this investigation are a uniform gust and a linearly distributed gust. Both environments are shown in Figure 5 and do not contain ship motion. Note that the angle of the wind above the horizon is α_w. The uniform gust distribution consists of a 40 knot gust with α_w=15 degrees. The linearly distributed gust is the same as the deterministic gust model developed in Ref. 7. The wind speed is 40 knots with a 25% upflow through the windward half of the rotor disk and a 25% downflow through the leeward half of the rotor disk. Both gusts approach from the starboard side of the aircraft (WOD direction = 090 degrees).

FLAP DAMPING STUDY

In an effort to reduce the frequency of tunnel strike occurrences, an investigation was conducted into the effectiveness of adding a rotational damper acting at the flap hinge of the H-46. Such a damper would dissipate energy in the flapping degree of freedom, much like the lead/lag damper dissipates energy in the lead/lag degree of freedom. Flap dampers have been used to reduce excessive blade flapping during low rotor speed operation on shipboard rotorcraft such as the HUP-1 through HUP-4 series helicopters as early as the 1950's [18].

H-46 rotor engagements were simulated in a 55 knot starboard wind using standard control inputs and a 25% linear gust fraction. Because the energy dissipated by the flap damper is proportional to the degree of hinge rotation it acts through, a range of flap stop settings from 1.5 degrees, the H-46's current flap stop setting, to 10 degrees was investigated. At

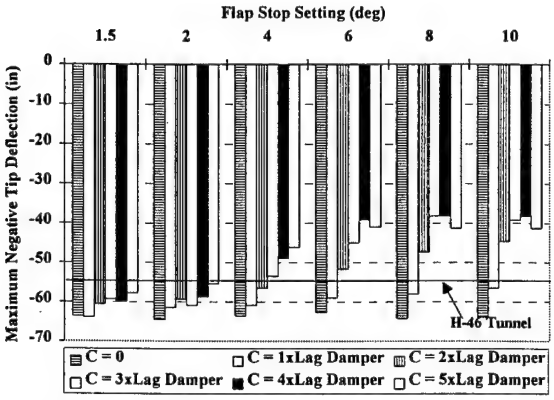

Figure 15: The effect of flap damping on the maximum downward tip deflection for various flap stop angles.

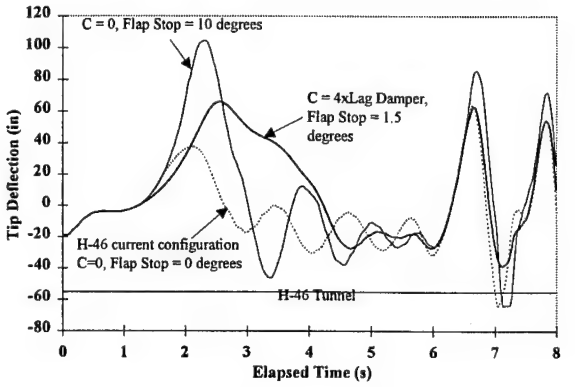

Figure 16: Tip deflection time histories for various flap stop angles and flap damping.

each flap stop setting, a range of flap damper strengths from zero, simulating the current H-46 configuration, to 5 times the lead/lag damper strength were tested. An effective damping value of 3500 ft-lb/(rad/s), typical for ground operations in the H-46, was assumed for the lead/lag damper strength.

Figure 15 shows the variation of the maximum negative tip deflection during each simulated engagement for the ranges of flap stop settings and flap damper strengths. At the current H-46 flap stop setting, only a reduction of 5.8 inches in the maximum negative tip deflection results even with the strongest dampers. Note that as the flap stop setting is raised and as the damping is increased, the maximum negative tip deflections decrease. If the flap stop setting is raised to 10 degrees and the flap damper is 4 times the strength of the lead/lag damper, the resulting tip deflection is -38.3 inches which is a 25.3 inch reduction from the analysis of the current H-46 configuration. For flap damping values 4 times the lead/lag damper, the tip deflections increased because the blade was prevented from flapping up far enough during the engagement.

Figure 16 shows the tip deflection time histories for rotor engagement with three flap stop settings and flap damper combinations. The maximum negative tip deflection occurred 7 seconds after engagement in all three configurations. With no flap damping, the maximum deflections are -63.6 inches and -64.0 inches, both tunnel strikes, at flap stop settings of 1.5 and 10 degrees respectively. At the flap stop setting of 10 degrees, note the excessive blade deflection. Early after engagement the rotor speed is low and with a lack of centrifugal stiffening any kinetic energy that the blade develops due to excessive flapping will be transferred to strain energy upon droop stop contact. If a flap damper 4 times the strength of the lead/lag damper is installed with an flap stop setting of 10 degrees, enough energy is dissipated to result in a 38.3 inch maximum tip deflection, preventing a tunnel strike in this simulation.

In summary, a tradeoff exists between flap damping and flap stop setting. With a low flap stop setting, neither can the blade flap to excessive angles developing much kinetic energy nor can the damper dissipate much energy acting through a small angle. At higher flap stop settings, the blade is allowed to develop extra kinetic energy transferred to strain energy upon droop stop contact; but the flap damper can dissipate more energy since it acts through a greater angle. Substantial tip deflection reductions occur only when the energy the flap damper dissipates becomes greater than the kinetic energy developed by the blade in excessive flapping. In the current H-46 configuration, this analysis suggests that the tip deflections cannot be reduced by a substantial amount no matter what the strength of the flap damper. However, if the flap stop is raised and a flap damper four times the strength of the lead/lag damper is used, tunnel strikes could be prevented.

BLADE START AZIMUTH STUDY FOR ROTOR ENGAGEMENT

There are few things the Navy can change while operating at sea to reduce the risk of a tunnel strike. The main concern since the emergence of tunnel strikes has been the wind-over-deck conditions. The ship would maneuver to obtain wind conditions that were favorable for a safe engage/disengage evolution. The azimuthal position of the blade before an engage sequence begins, the blade start azimuth, can also be adjusted to reduce the risk of a tunnel strike. This study explores trends in both maximum downward tip deflections and blade strike azimuth

due to variations in WOD direction. Blade strike azimuth refers to the azimuthal position of the blade where maximum tip deflection occurs.

This study is completed for rotor engagements only and uses the baseline H-46 model with standard control inputs. The wind is uniformly distributed with α_w=15 degrees. The rotor is engaged under four wind directions, 000, 090, 180, and 270 degrees, for a wind speed of 40 knots. The blade is started at eight azimuth positions. In some of the results shown below, the blade start azimuth is referenced to the WOD direction. An illustration of this convention is shown in Figure 17. For this example, the wind direction is 270 degrees. Note the positive angles of the blade azimuth relative to the WOD direction increase in the direction of the rotor rotation.

The maximum downward tip deflections as a function of the strike azimuth referenced to the start azimuth are illustrated in Figure 18. Note that the trends for every WOD direction show a distinct trough; however the lowest point for the WOD direction of 090 does not agree with the trend of the other points for that WOD direction. The lowest maximum downward tip deflection for a WOD direction of 090 occurs within 5 degrees of the start azimuth. The trends of the other three WOD directions suggest the lowest maximum downward tip deflection occurs approximately 240 and 300 degrees from the start azimuth; therefore, as long as any one blade is not positioned over the tunnel or between 240 to 300 degrees before the tunnel, the lowest maximum downward tip deflections do not occur over the tunnel.

The strike azimuths relative to the WOD direction as a function of the start azimuth referenced

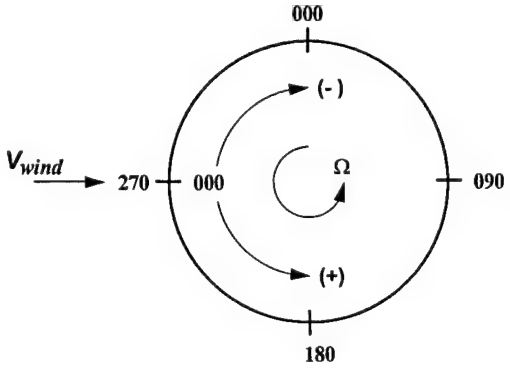

Figure 17: Graphical explanation of the blade azimuth relative to the WOD direction.

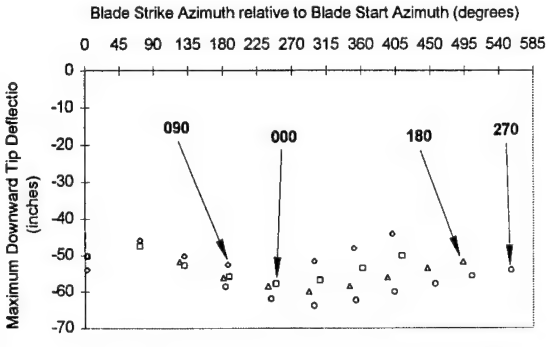

Figure 18: Start azimuth effects on maximum downward tip deflections for various WOD directions.

to the WOD direction are shown in Figure 19. Note that strike azimuths for WOD directions of 180 and 270 occur between 55 degrees before and 15 degrees after the WOD direction; however, the strike azimuths for WOD directions of 000 and 090 range from 90 degrees before to 90 degrees after the WOD direction. These results suggest that engaging in winds with WOD directions from 100 to 260 regardless of the start azimuth guarantees the strike azimuth is not over the tunnel. Also note that all of the WOD directions agree that the strike azimuth occurs within 25 degrees before the WOD direction for the blade started between 0 and 90 degrees relative to the WOD direction.

ENGAGE ENVELOPE STUDY

As stated earlier, the likeliness of a blade strike is determined primarily by the WOD conditions. The WOD conditions conducive to safe engage/disengage evolutions are graphically illustrated in engage/disengage envelopes. Maximum downward tip deflections are classified according to the blade

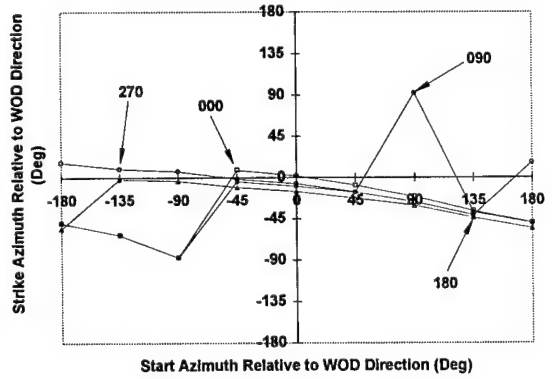

Figure 19: Start azimuth effects on strike azimuth for various WOD directions.

clearance scale outlined by the Navy. Details of this classification process are described in the analysis section. This analysis does not consider the azimuthal position of the blade when classifying the severity of the tip deflection.

An H-46 baseline engagement envelope developed using standard control inputs and a uniformly distributed gust with α_w = 15 degrees is shown in Figure 20. Note that the H-46 is limited to wind speeds of 30 knots for port WOD conditions and is limited to 35 knots for most starboard WOD conditions. However the predicted envelope shows safe engagements for winds speeds up to 40 knots for WOD directions of 045 to 075 degrees. Results of sensitivity studies presented in Ref. 10 showed control inputs to have a moderate effect on maximum downward tip deflections. The present research investigates the effects of 2 degree variations from the standard lateral cyclic and collective control inputs on the H-46 engage envelope. The predicted H-46 engage envelope for a collective input of 1 degree is shown in Figure 21. A comparison with the baseline H-46 engage envelope shows a 5 knot reduction in the safe engagement region for WOD directions of 045 to 075 degrees and 120 to 285 degrees. This results in 14.5% reduction in the H-46 engagement capability. The predicted H-46 engage envelope for a lateral cyclic input of 2 degrees is shown in Figure 22. Note the substantial reduction in engagement capability for port winds. WOD speeds are reduced by 10 to 15 knots for WOD directions of 120 to 150 degrees and 225 to 330 degrees. There was a small 5 knot increase in the safe engage region

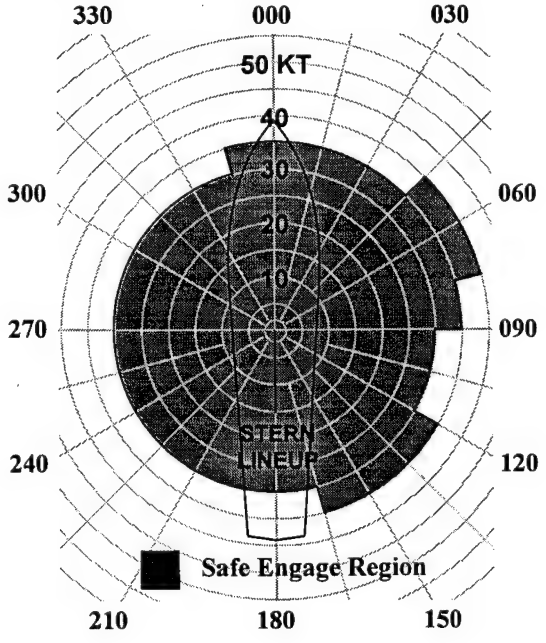

Figure 20: H-46 engage envelope for the uniform WOD condition and standard control inputs.

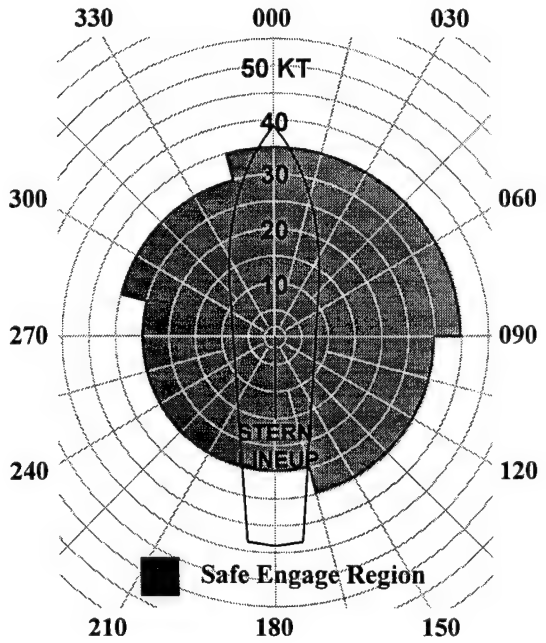

Figure 21: H-46 engage envelope for uniform WOD conditions and a collective input of 1 degree.

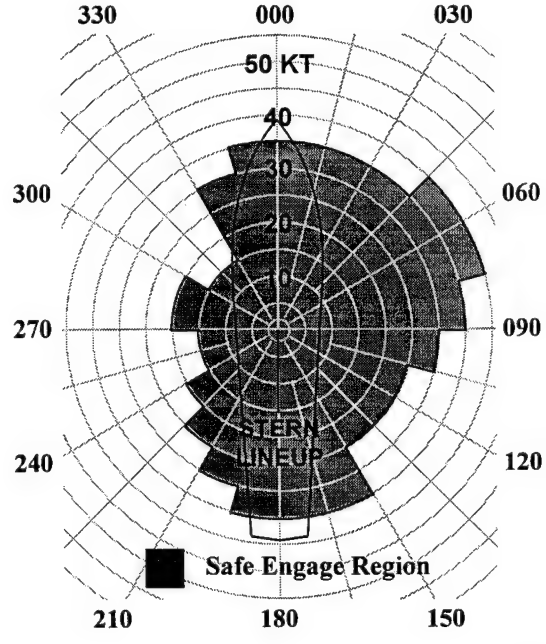

Figure 22: H-46 engage envelope for uniform WOD conditions and a lateral cyclic input of 2 degrees.

for stern winds from 165 to 195 degrees. The 2 degree change in lateral cyclic resulted in a 20.7% reduction in the safe engage region. These results illustrate that control input changes can adversely impact the safe engage region for a uniformly distributed wind with $\alpha_w = 15$ degrees.

RUN-UP/RUN-DOWN ROTOR SPEED PROFILE STUDY

The present analysis is capable of computing a transient rotor response for an arbitrary rotor speed time history. The H-46 engage rotor speed profile developed with limited experimental data is shown in Figure 14 and provides a general trend to examine rotor response in the present research. In this study, the run-up models are developed strictly from CH-46E experimental data and the run-down rotor speed models are developed from a combination of analytics and CH-46E experimental data. The following paragraphs discuss the development of the H-46 run-up/run-down rotor speed profiles for a range of pilot techniques and presents the effects of the pilot techniques on transient blade response.

A continuing effort is being conducted by NAWC-AD, Pax River, to determine the experimental engage/disengage rotor speed variations. The H-46 rotor hub is filmed using an 8mm home video camera and variations of rotor blade passage with time are determined. During rotor engagement, the only procedure the pilot can vary is the advancement speed of the engine throttles. The effects of throttle advancement rate on the run-up rotor speed profile is shown in Figure 23. The average rotor speed for each blade pass is plotted and very sparse data is provided for rotor speeds below 5 percent due to the measurement technique. Run-up 1 corresponds to the slowest advancement of the engine throttles while run-up 4 corresponds to the fastest advancement of the throttles. Using these engage rotor speed profiles, the maximum downward tip deflections are computed for the baseline uniform and linear gust distributions and the results are shown in Figure 24. Note that the results for the uniform gust distribution are insensitive to engine throttle advancement rate. In contrast, the maximum downward tip deflections differ by approximately 8 inches between the fastest and slowest throttle advancement rate for the linear gust distribution. The latter prediction supports the conclusions of Ref. 1 that faster throttle advancement reduces the chances of a tunnel strike.

The difference in maximum downward tip deflection sensitivity to the gust distribution is explained by the characteristic response of the rotor blade to a particular gust distribution. Ref. 10 illustrated typical rotor responses for the uniform and linear gust distributions. It was concluded that the maximum downward tip deflections for a uniform gust distribution were caused by the downward lifting force of the blade and little blade/droop stop interaction and vice-versa for linearly distributed gusts. The results from this analysis show maximum downward tip deflections for the uniform gust distribution occur at rotor speeds less than 10 percent and the maximum tip deflections for the linear gust distribution occur at rotor speeds between 10 and 20 percent. Maximum downward tip deflections occurring at lower rotor speed regions for the uniform gust distribution suggests that the downward lifting force of the blade is not sufficient to overcome the centrifugal forces at higher rotor speeds. Conversely, the dynamic nature of the blade response subjected to linear gust distribution enables the blade to reach maximum downward tip deflections at higher rotor speeds.

Unlike rotor engagement, the rotor speed

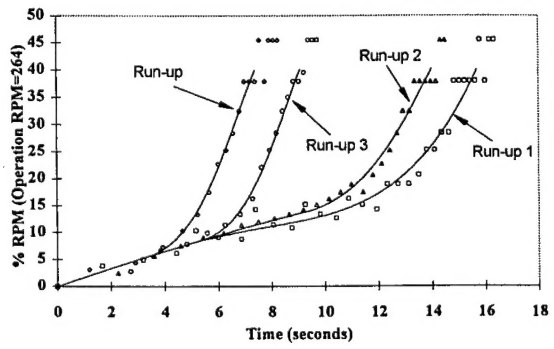

Figure 23: Effects of throttle advancement on H-46 run-up rotor speed profiles.

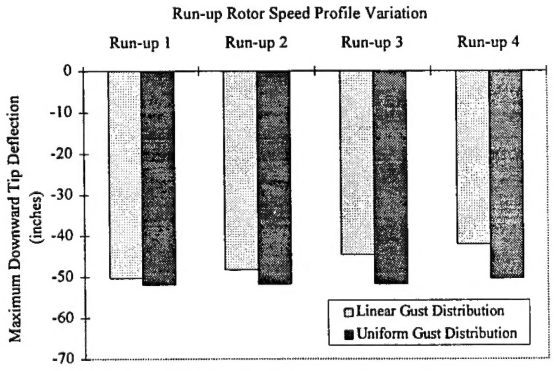

Figure 24: Effects of run-up variations on maximum downward tip deflections.

profiles for disengagement require the rotor speed variation between 50 and 100 percent provide physically real initial conditions. The run-down sequence has three phases; the settling phase, the freely spinning phase, and the braking phase. The first phase is the settling phase which allows the numerical scheme to reach a steady state response for a constant rotor speed of 100%. The blade response solution converges to a steady state condition within one second. The second phase models the rotor freely spinning after the throttle is cut and before the rotor brake is applied (T_{brake}=0). The rotor speed measurement technique could not accurately estimate rotor speed variations higher than 50 percent; therefore, a simple analytic model was developed to predict the freely spinning phase. The differential equation that governs the rotational speed of the rotor system during this phase is expressed as

$$J\dot{\Omega} = -T_{drag} \tag{16}$$

where T_{drag} is the torque due to aerodynamic drag. The drag torque is assumed to vary with the square of the rotor speed and can be express as

$$T_{drag} = C_{drag}\Omega^2 \tag{17}$$

where C_{drag} is a constant which is estimated using experimentally determined time constants. The braking phase uses experimental data to estimate the rotor speed variation.

Disengagement rotor speed profiles representative of the CH-46E are shown in Figure 25 along with the experimental rotor speed data used to determine the braking phase. The only procedure the pilot can vary in the run-down sequence is the rotor speed at which the rotor brake is applied. The pilots are only allowed to apply the rotor brake between 65 and 45 percent operational rotor speed. The experimental data shown in Figure 25 represents the rotor system response to various brake application

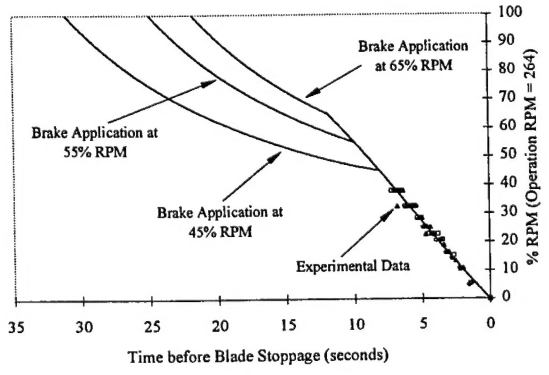

Figure 25: Effects of brake application rotor speed on H-46 run-down rotor speed profiles.

rotor speeds. Note that the slope of the experimental data remains consistent between the different sets of data; therefore, only one curve is faired through the data. The run-down portion of this study presents results for variations in rotor speeds at which the rotor brake was applied. The effects of rotor speed run-down variation on maximum downward tip deflection for the uniformly and linearly distributed gusts are shown in Figure 26. Note that for both gust distributions, the maximum downward tip deflections are insensitive to the rotor speed for rotor brake application; therefore, this study suggests that maximum downward tip deflection is independent of pilot procedure. Further studies of experimentally determined disengage rotor speed profiles should be conducted to verify the disengage rotor speed profiles used in this investigation.

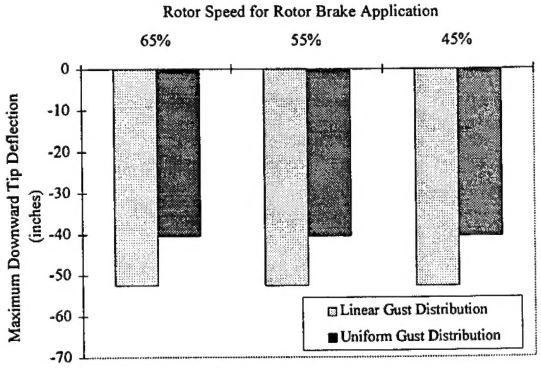

Figure 26: Effects of H-46 run-down variations on maximum downward tip deflections.

CONCLUSIONS

A previously developed transient aeroelastic rotor response analysis for shipboard engage/disengage sequences is utilized in the present research. This analysis is modified to include a flap stop which restrains upper flap motion and a flap damper which damps flap hinge motion. In addition, an arbitrary gust model is incorporated into the analysis to enable more realistic airwake models. The enhanced capabilities are used to conduct a validation with scale rotor system model and investigate the effects of pilot controllable parameters on the risk of H-46 tunnel strikes. In addition, the feasibility and effectiveness of incorporating flap damping at the blade root is investigated.

1) A comparison is performed between the present analysis and experimental results of a scale model rotor system placed in a wind tunnel. The experimental results were collected for five positions

of the rotor system resting on a simulated flight deck. The measured average values of the airwake variation over the rotor disk are used in the theoretical analysis. Theoretical predictions are shown to be in good agreement with experimental results for the most windward and center positions on the flight deck. However, theoretical predictions did not agree very well with experimental results for the most leeward deck position which is attributed to the absence of a temporally varying airwake model.

2) When the hub is positioned in the windward deck positions, the validation also revealed differences in blade response calculated using unsteady aerodynamics and quasi-steady aerodynamics. This suggests that blade response calculations for windward deck positions may require a higher fidelity aerodynamic model.

3) In the current flap stop configuration, a flap damper would not be effective in reducing the maximum downward tip deflections due to the small allowable flap hinge rotation angle. The present research suggests that a flap damper may be effective and feasible if the flap stop angle is raised.

4) The start azimuth is shown to have a significant impact on the blade response for uniform WOD conditions. In particular, the results suggest that an H-46 may safely engage at any start azimuth if the WOD direction is between 100 and 260 degrees.

5) Pilot control inputs can adversely impact the predicted H-46 engage envelopes under uniform WOD conditions.

6) Faster throttle advancement is shown to reduce the maximum downward tip deflection for linear distributed gusts due to the characteristically high droop stop/blade interaction.

7) Assuming similar deceleration profiles for the braking phase of disengagement, the maximum downward tip deflection is shown to be insensitive to the rotor speed at which the rotor brake is applied for both gust distributions. This suggests that the maximum downward tip deflections are independent of pilot procedure for H-46 disengagement sequences.

ACKNOWLEDGMENTS

This research was carried out with support from the Naval Air Warfare Center at Patuxent River, Maryland (technical monitors: LCDR Mark Whittle, Mr. Kurt Long, and Mr. Larry Trick) and Naval Aviation Depot at Cherry Point, North Carolina (technical monitor: Maj. Heller). The authors are also grateful to Mr. George Thompson, Mr. William Harris, and Mr. John Kannon of Boeing Helicopters for providing technical information on the H-46 Sea Knight rotor system and Mr. S.J. Newman of the University of Southampton, U.K. for providing scale model transient rotor response data.

REFERENCES

1. Carico, G.D., J.W. Groulx, and D.R. Vetter, "H-46 Rotor Engage/Disengage Evaluation Aboard the USS GUADALCANAL (LPH-11)," NAVAIRTESTCEN Report of Test Results FT-49R-74, 18 June 1974.

2. Fowler, J.E., P.W. Martin, and L.L. Trick, "H-46 Dynamic Interface Tests Aboard USS WABASH (AOR-5)," NAVAIRTESTCEN Technical Report RW-94R-84, 4 June 1985.

3. Ball, J.C. and W.R. White, "H-46 Dynamic Interface Tests Aboard USS GUAM (LPH-9)," NAVAIRTESTCEN Technical Report RW-28R-83, 29 March 1984.

4. Hurley, G.E., C.W. Pittman, and L.L. Trick, "HH-46A/CV-64 Rotor Engage/Disengage Test," NAVAIRTESTCEN Report of Test Results RW-55R-84, 30 October 1984.

5. Ruffa, S.A. and E.C. Traasdahl, "CH-46E/ LHA-4 Engage/Disengage Dynamic Interface Test," NAVAIRTESTCEN Report of Test Results RW-58R-84, 30 January 1985.

6. Hurst, D.W. and S.J. Newman, "Wind Tunnel Measurements of Ship Induced Turbulence and the Prediction of Helicopter Rotor Blade Response," Eleventh European Rotorcraft Forum Paper No. 99, 10-13 September 1985.

7. Newman, S.J., "A Theoretical Model for Predicting the Blade Sailing Behaviour of a Semi-Rigid Rotor Helicopter," *Vertica*, Vol. 14, No. 4, pp. 531-544, 1990.

8. Newman, S.J., "The Application of a Theoretical Blade Sailing Model to Predict the Behaviour of Articulated Helicopter Rotors," *The Aeronautical Journal of the Royal Aeronautical Society*, June/July 1992.

9. Newman, S.J., "An Investigation into the Phenomenon of Helicopter Blade Sailing," University of Southampton, United Kingdom, March 1995.

10. Geyer, W. P., "Aeroelastic Analysis of Transient Blade Dynamics during Shipboard Engage/ Disengage Operations," Pennsylvania State University Thesis, August 1995.

11. Smith, E.C., "Aeroelastic Response and Aeromechanical Stability of Helicopters with Elastically Coupled Composite Rotor Blades," University of Maryland Thesis, UM-AERO 92-15, 31 July 1992.

12. Ferrier, B. and J. Semenza, "NATC Manned Flight Simulator VTOL Ship Motion Simulation and Application," Presented at the 46th Annual National Forum of the American Helicopter Society, Washington, D.C., May 1990.

13. Johnson, W., *Helicopter Theory*, Dover Publications, Inc., New York, 1994.

14. Bir, G. and Inderjit Chopra, "University of Maryland Advanced Rotorcraft Code (UMARC) Theory Manual," University of Maryland, UM-AERO 92-02, College Park, MD, 7 August 1992.

15. Beddoes, T.S. and J.G. Leishman, "A Generalised Model for Airfoil Unsteady Aerodynamic Behavior and Dynamic Stall using the Indicial Method," Presented at the 42nd. Annual Forum of the American Helicopter

16. Beddoes, T.S. and J.G. Leishman, "A Semi-Empirical Model for Dynamic Stall," *Journal of the American Helicopter Society*, July 1989.

17. Leishman, J.G., *Unsteady Aerodynamic Theory Manual for the Technology Complex (TC) Airloads and Induced Velocity (ALIV) CPCI of the Second Generation Comprehensive Helicopter Analysis (2GCHAS)*, University of Maryland, College Park, July 1990.

18. Lemont, H.E., "Rotor Blade Flapping Control Mechanism, Patent No. 2,946,391," United States Patent Office, Filed 29 December 1955, Patented 26 July 1960.